# Cyclotron resonance of an interacting polaron gas in a quantum well: Magnetoplasmon-phonon mixing

S. N. Klimin* and J. T. Devreese†
*Theoretische Fysica van de Vaste Stoffen, Universiteit Antwerpen, B-2610 Antwerpen, Belgium*
(Received 18 June 2003; published 5 December 2003)

Cyclotron-resonance (CR) spectra of a gas of interacting polarons confined in a GaAs/AlAs quantum well are theoretically investigated taking into account the magnetoplasmon-phonon mixing and band nonparabolicity. Contributions of different magnetoplasmon-phonon modes to the total magnetopolaron coupling strength are investigated as a function of the electron density. It is confirmed theoretically, that the resonant magnetopolaron coupling in a high-density GaAs/AlAs quantum well occurs near the GaAs TO-phonon frequency rather than near the GaAs LO-phonon frequency. Calculated CR spectra are in agreement with recent experimental data.

DOI: 10.1103/PhysRevB.68.245303 PACS number(s): 78.67.De, 71.38.−k, 78.30.Fs

## I. INTRODUCTION

The electron-LO-phonon interaction plays an important role in the optical properties of polar semiconductors and ionic crystals (see, for review, Refs. 1–5). The application of an external magnetic field adds new features to the optical absorption spectra of these materials. When the cyclotron frequency $\omega_c$ is close to the LO-phonon frequency, resonant magnetopolaron coupling (i.e., anticrossing of zero-phonon and, e.g., one-phonon states of the polaron system) occurs.[6] Experiments on the cyclotron resonance (CR) in bulk[7] and quasi-two-dimensional (2D) (Refs. 8–10) systems give clear evidence of this resonant magnetopolaron coupling. However, CR measurements on semiconductor quantum wells with high electron density[11,12] reveal that the anticrossing occurs near the TO-phonon frequency rather than near the LO-phonon frequency. In Ref. 12, on the basis of a model dielectric function for a 3D medium, it was suggested that in a GaAs/AlAs quantum well with high electron density, there may exist longitudinal modes, with energies close to the TO-phonon frequency, which are active in CR.

Another consequence of high electron densities combined with the nonparabolicity of the conduction band is a splitting of the CR lines.[13–17] It was shown in Ref. 16, that the one-particle approximation fails to interpret the oscillator strengths of the split CR lines.

Many-polaron CR in a 2D polaron gas was investigated theoretically in Ref. 18 using the memory-function technique.[19] In Ref. 10, this technique was applied to a polaron gas in a quantum well. The CR spectra of polarons in a quantum well were calculated in Refs. 20–22 and applied in Refs. 23, 24 taking into account the electron-phonon interaction for both bulklike and interface phonon modes.[25–28] To quantitatively explain the CR data for a high-density polaron gas, as observed in Ref. 12, it is necessary to take into account many-body effects.

In the present paper, the CR spectra of an arbitrary-density polaron gas in a quantum well are calculated using the many-body memory-function technique.[19] The approach developed in Refs. 18, 21 is extended here to a system of electrons confined in a quantum well and interacting with magnetoplasmon-phonon modes. Within this method, we take into account the electron-electron interaction, the static and dynamic screening of the electron-phonon interaction,[18] the magnetoplasmon-phonon mixing,[29] the band nonparabolicity, and the optical-phonon spectra specific for a quantum well.

The paper is organized as follows. In Sec. II, the optical conductivity for a polaron gas in a quantum well is derived. In Sec. III, we discuss the calculated CR spectra and compare them with experimental data for a GaAs/AlAs quantum well. Section IV contains the conclusions.

## II. THEORETICAL APPROACH

### A. Hamiltonian

We consider a finite-barrier quantum well of width $d$. The quantum well (medium 1) with high-frequency dielectric constant $\varepsilon_1$ is placed into a matrix (medium 2) with high-frequency dielectric constant $\varepsilon_2$. Both these media are supposed to be polar. An external magnetic field $\mathbf{B}$ is applied parallel to the $z$ axis. The symmetric gauge is chosen for the vector potential of the magnetic field

$$\mathbf{A}(\mathbf{r}) = \tfrac{1}{2}[\mathbf{r}\times\mathbf{B}]. \tag{1}$$

The Hamiltonian describing the system, which consists of electrons interacting with phonons and with each other, is

$$\begin{aligned} H = & \sum_{nlm\sigma} E_{nl\sigma} a^{+}_{nlm\sigma} a_{nlm\sigma} + \sum_{\lambda,\mathbf{q}} \hbar\omega_{\lambda,\mathbf{q}} b^{+}_{\lambda,\mathbf{q}} b_{\lambda,\mathbf{q}} \\ & + \frac{1}{\sqrt{S}} \sum_{\lambda,\mathbf{q}} \sum_{n,k} (\gamma_{\lambda,\mathbf{q}})_{nk} \rho_{nk}(\mathbf{q}) (b_{\lambda,\mathbf{q}} + b^{+}_{\lambda,-\mathbf{q}}) \\ & + \frac{1}{2S} \sum_{\mathbf{q}} \sum_{n_1 k_1 n_2 k_2} V_C(k_1, n_1; n_2, k_2 | \mathbf{q}) \\ & \times \mathcal{M}[\rho^{+}_{k_1 n_1}(\mathbf{q}) \rho_{n_2 k_2}(\mathbf{q})], \end{aligned} \tag{2}$$

where $a^{+}_{nlm\sigma}(a_{nlm\sigma})$ is a creation (annihilation) operator for an electron in the one-particle state with energy $E_{nl\sigma}$ and with the wave function

 

$$\Psi_{nlm}(\rho,\varphi,z)=\psi_n(z)\phi_{lm}(\rho,\varphi),$$

$$\phi_{lm}(\rho,\varphi)=\frac{1}{\sqrt{2\pi}}e^{im\varphi}\Phi_{lm}(\rho). \tag{3}$$

Here, the function $\psi_n(z)$ corresponds to the $n$th size-quantized subband for motion along the $z$ axis, while $\phi_{lm}(\rho,\varphi)$ characterizes the ''in-plane'' motion of an electron with a definite $z$ projection $m$ of its angular momentum, $l$ is the Landau level quantum number.

The phonon frequencies $\omega_{\lambda,\mathbf{q}}$ and the amplitudes of the electron-phonon interaction $\gamma_{\lambda,\mathbf{q}}$ are explicitly derived in Refs. 21, 28. The index λ refers to the phonon branches, $\mathbf{q}$ is the phonon two-dimensional wave vector, $b^+_{\lambda,\mathbf{q}}(b_{\lambda,\mathbf{q}})$ is a phonon creation (annihilation) operator. $\rho_{nk}(\mathbf{q})$ is the electron density operator

$$\rho_{nk}(\mathbf{q})=\sum_{lml'm'\sigma}(e^{i\mathbf{q}\cdot\mathbf{r}_\parallel})_{lm,l'm'}\hat{a}^+_{nlm\sigma}\hat{a}_{kl'm'\sigma} \tag{4}$$

with the matrix element

$$(e^{i\mathbf{q}\cdot\mathbf{r}_\parallel})_{lm,l'm'}=\int_0^\infty\rho d\rho\int_0^{2\pi}d\varphi e^{i\mathbf{q}\cdot\mathbf{r}_\parallel}\phi^*_{lm}(\rho,\varphi)\phi_{l'm'}(\rho,\varphi). \tag{5}$$

In the Hamiltonian (2), $V_C(k_1,n_1;n_2,k_2|\mathbf{q})$ is the matrix element of the electron-electron interaction potential

$$V_C(k_1,n_1;n_2,k_2|\mathbf{q})=\int_{-\infty}^{\infty}dz\int_{-\infty}^{\infty}dz'\times\tilde{V}_C(\mathbf{q};z,z')\psi^*_{k_1}(z)\times\psi_{n_1}(z)\psi^*_{n_2}(z')\psi_{k_2}(z'), \tag{6}$$

$S$ is the area of the quantum well in the $xy$ plane, $\mathcal{N}[\cdots]$ is a normal product of operators. The two-dimensional Fourier amplitude $\tilde{V}_C(\mathbf{q};z,z')$ of the electron-electron interaction potential, specific for a quantum well,

$$\tilde{V}_C(\mathbf{q};z,z')=\frac{2\pi e^2}{\varepsilon_1 q}e^{-q|z-z'|}+\frac{2\pi e^2(\varepsilon_1-\varepsilon_2)}{\varepsilon_1 q}\frac{(\varepsilon_1+\varepsilon_2)\cosh[q(z+z')]+(\varepsilon_1-\varepsilon_2)e^{-qd}\cosh[q(z-z')]}{[\varepsilon_1^2+\varepsilon_2^2+2\varepsilon_1\varepsilon_2\coth(qd)]\sinh(qd)}, \tag{7}$$

differs from the corresponding expression for the Coulomb potential in bulk $[(2\pi e^2/\varepsilon q)e^{-q|z-z'|}]$ owing to the presence of the electrostatic image forces, which appear as long as $\varepsilon_1\neq\varepsilon_2$ (see, e.g., Refs. 30–32). The potential (7) is analytically exact within the dielectric-continuum approach.

Within the local parabolic band approximation,[33,34] nonparabolicity is considered as a small perturbation. Consequently, the wave function $\Phi_{lm}(\rho)$ (3) for an electron in a magnetic field takes the form

$$\Phi_{lm}(\rho)=\sqrt{\frac{2K!}{(|m|+K)!}}\left(\frac{m_b\omega_c}{2\hbar}\right)^{(|m|+1)/2}\rho^{|m|}\times\exp\left(-\frac{m_b\omega_c}{4\hbar}\rho^2\right)L_K^{(|m|)}\left(\frac{m_b\omega_c}{2\hbar}\rho^2\right),$$
$$K=l-\frac{m+|m|}{2},\quad m=-\infty,\ldots,l \tag{8}$$

with the Laguerre polynomial $L_K^{(a)}(z)$. Here, the cyclotron frequency $\omega_c=eB/(m_bc)$ corresponds to the mass $m_b$ given by[21]

$$m_b=\frac{m_{b1}m_{b2}}{P_wm_{b2}+P_bm_{b1}}, \tag{9}$$

where $P_w(P_b)$ is the probability to find the electron inside (outside) the quantum well, and $m_{bi}$ $(i=1,2)$ is the electron band mass at the bottom of the conduction band in the $i$th medium. The energies of the spin-dependent electron states are

$$E_{nl\sigma}=E_{nl}+g\mu_BB\sigma, \tag{10}$$

where $g$ is the Landé factor, $\mu_B$ is the Bohr magneton, and $\sigma=\pm1/2$ is the spin projection. The energy levels $E_{nl}$ corresponding to the wave functions $\Psi_{nlm}(\rho,\varphi,\dot{z})$ in (3) are calculated using the five-band $\mathbf{k}\cdot\mathbf{p}$ model.[35]

### B. Optical conductivity

Within the memory-function formalism, the real part of the frequency-dependent conductivity (in the Faraday configuration) in the local parabolic band approximation, can be written as[18,34]

$$\mathrm{Re}\,\sigma(\omega)=-\frac{n_Se^2}{m_b}\mathrm{Im}\frac{1}{\omega-\omega_c-\chi(\omega,\omega_c)/\omega+i\delta}(\delta\to+0), \tag{11}$$

where $n_S$ is the 2D electron density and $\chi(\omega)$ is the memory function.[18] To take into account the splitting of the CR peaks due to the *nonparabolicity* of the conduction band, Eq. (11) is generalized as follows:

$$\mathrm{Re}\,\sigma(\omega)=\sum_{n,l,\sigma}\varkappa_{nl\sigma}\,\mathrm{Re}\,\sigma_{nl\sigma}(\omega). \tag{12}$$

where each contribution $\mathrm{Re}\,\sigma_{nl\sigma}(\omega)$, corresponding to the transitions $(l\to l+1)$,

$$\mathrm{Re}\,\sigma_{nl\sigma}(\omega)=-\frac{n_S e^2}{m_b}\mathrm{Im}\frac{1}{\omega-\omega_c^{(nl\sigma)}-\chi(\omega,\omega_c^{(nl\sigma)})/\omega+i\delta} \quad (\delta\to+0) \tag{13}$$

is calculated with the local parabolic band approximation. The transition frequency

$$\omega_c^{(nl\sigma)}\equiv\frac{E_{n,l+1,\sigma}-E_{nl\sigma}}{\hbar} \tag{14}$$

is used in Eq. (13) as distinct from the cyclotron frequency $\omega_c$ in Eq. (11). The weight $\varkappa_{nl\sigma}$ is proportional to the number of open channels for the transitions $(l\to l+1)$. The normalized weights $\varkappa_{nl\sigma}$ are

$$\varkappa_{nl\sigma}=\frac{f_{nl\sigma}(1-f_{n,l+1,\sigma})}{\Sigma_{n',l',\sigma'}f_{n'l'\sigma'}(1-f_{n',l'+1,\sigma'})}, \tag{15}$$

where $f_{nl\sigma}$ is the Fermi occupation number. The memory function $\chi(\omega,\omega_c)$ takes the form (see Refs. 18, 21)

$$\chi(\omega,\omega_c)=-\sum_{n,k}\sum_{\lambda}\int\frac{d^2\mathbf{q}}{(2\pi)^2}\frac{|(\gamma_{\lambda,\mathbf{q}})_{nk}|^2q^2}{n_S\hbar m_b\epsilon^2(q)}\times\int_0^\infty dt e^{-\delta t}(e^{i\omega t}-1)\mathrm{Im}[\mathcal{D}_\lambda(\mathbf{q},t)G_{nk}(\mathbf{q},t)] \quad (\delta\to+0), \tag{16}$$

where $\epsilon(q)$ is the static screening factor.[18] $\mathcal{D}_\lambda(\mathbf{q},t)$ is the phonon Green's function

$$\mathcal{D}_\lambda(\mathbf{q},t)\equiv-i\Theta(t)[\langle b_{\lambda,\mathbf{q}}(t)b^+_{\lambda,\mathbf{q}}(0)\rangle+\langle b^+_{\lambda,-\mathbf{q}}(t)b_{\lambda,-\mathbf{q}}(0)\rangle] \tag{17}$$

and $G_{nk}(\mathbf{q},t)$ is the electron density-density Green's function

$$G_{nk}(\mathbf{q},t)=-i\Theta(t)\frac{1}{S}\langle\rho_{nk}(\mathbf{q},t)\rho^+_{nk}(\mathbf{q},0)\rangle \tag{18}$$

with the Heaviside step function $\Theta(t)$. The averaging in Eqs. (17) and (18) is performed on the equilibrium statistical operator of the electron-phonon system.

In the present paper, we apply the method presented above to the case of a GaAs/AlAs quantum well, where the weak-coupling regime is realized. To obtain $\chi(\omega,\omega_c)$ to second order in perturbation theory, the electron density-density Green's function $G_{nk}(\mathbf{q},t)$ can be calculated neglecting the electron-phonon interaction. The electron-electron interaction is taken into account in the random-phase approximation (RPA) following Ref. 36, where plasmon modes are derived for electrons in a layer. As a result, we arrive at the following set of equations in the Fourier representation:

$$\sum_{n_1k_1}[\delta_{nn_1}\delta_{kk_1}-P_{nk}(\mathbf{q},\omega)V_C(k,n;k_1,n_1|\mathbf{q})]G^R_{n_1k_1,\tilde{n}\tilde{k}}(\mathbf{q},\omega)=\delta_{n,\tilde{n}}\delta_{k\tilde{k}}\hbar P_{nk}(\mathbf{q},\omega). \tag{19}$$

Here, the auxiliary retarded Green's function $G^R_{nk,\tilde{n}\tilde{k}}(\mathbf{q},\omega)$ is determined as

$$G^R_{nk,\tilde{n}\tilde{k}}(\mathbf{q},\omega)\equiv-\frac{i}{S}\int_0^\infty\langle[\rho_{nk}(\mathbf{q},t),\rho^+_{\tilde{n}\tilde{k}}(\mathbf{q},0)]\rangle e^{i\omega t-\delta t}dt \quad (\delta\to+0). \tag{20}$$

The RPA structure factor $P_{nk}(\mathbf{q},\omega)$ is proportional to the retarded density-density Green's function of noninteracting electrons in the quantum well in the presence of a magnetic field. It is calculated explicitly, using the second-quantization representation of the density operators (4), and takes the form

$$P_{nk}(\mathbf{q},\omega)=-i\frac{m_b\omega_c}{2\pi\hbar^2}\int_0^\infty dt\exp[i(\omega-\omega_{kn})t-\delta t]\times\sum_{l\sigma}L_l^{(0)}\left(\frac{\hbar q^2}{m_b\omega_c}(1-\cos\omega_c t)\right)\times\left(f_{nl\sigma}\exp\left[-\frac{\hbar q^2}{2m_b\omega_c}(1-e^{-i\omega_c t})\right]-f_{kl\sigma}\exp\left[-\frac{\hbar q^2}{2m_b\omega_c}(1-e^{i\omega_c t})\right]\right) \quad (\delta\to+0), \tag{21}$$

where $\omega_{kn}$ is the transition frequency between the $k$th and $n$th size-quantized subbands.

The set of equations (19) is valid for arbitrary electron density. The Green's function $G_{nk}(\mathbf{q},\omega)$ is obtained from $G^R_{nk}(\mathbf{q},\omega)$ using the Kramers-Kronig dispersion relations and the relation, which follows from the analytical properties of Green's functions

$$\mathrm{Im}\,G^R_{nk}(\mathbf{q},\omega)=(1-e^{-\beta\omega})\mathrm{Im}\,G_{nk}(\mathbf{q},\omega), \tag{22}$$

where $\beta\equiv1/(k_BT)$. Further on, we consider the case of a sufficiently narrow quantum well, when only the lowest size-quantization subband $(n=1)$ is filled, and the transition frequency $\omega_{21}\gg\omega_{Li}$, where $\omega_{Li}$ is the LO-phonon frequency in the $i$th medium $(i=1,2)$. Under these conditions, transitions of an electron to other subbands can be neglected. This results in the explicit solution

$$G^R_{11}(\mathbf{q},\omega)=\frac{\hbar P_{11}(\mathbf{q},\omega)}{1-V_C(\mathbf{q})P_{11}(\mathbf{q},\omega)} \tag{23}$$

with $V_C(\mathbf{q})\equiv V_C(1,1;1,1|\mathbf{q})$.

The phonon retarded Green's function is calculated within the random-phase approximation taking into account the magnetoplasmon-phonon mixing (see Ref. 29). In the present case of a narrow quantum well, we take into account the mixing of phonons with intrasubband magnetoplasmons only. In this approximation, disentangling a set of coupled Dyson equations leads to

$$\mathcal{D}^R_\lambda(\mathbf{q},\omega)=\frac{2\left(\omega_{\lambda,q}+\dfrac{|(\gamma_{\lambda,q})_{11}|^2}{\hbar^2}G^R_{11}(\mathbf{q},\omega)\right)}{(\omega+i\delta)^2-\omega^2_{\lambda,q}-2\omega_{\lambda,q}\dfrac{|(\gamma_{\lambda,q})_{11}|^2}{\hbar^2}G^R_{11}(\mathbf{q},\omega)}$$

$$(\delta\to+0). \tag{24}$$

The poles of this Green's function are the roots of the equation

$$\omega^2-\omega^2_{\lambda,q}-2\omega_{\lambda,q}\frac{|(\gamma_{\lambda,q})_{11}|^2}{\hbar^2}\mathrm{Re}\,G^R_{11}(\mathbf{q},\omega)=0 \tag{25}$$

and they determine the spectrum of mixed magneto-plasmon-phonon excitations in the quantum well. Let $\Omega_{\lambda,j}(\mathbf{q})$ denote the positive roots of Eq. (25). Using $G^R_{11}(\mathbf{q},\omega)$ given by Eq. (23), with the structure factor (21), we find that the retarded Green's function (24) can be expanded as a series

$$\mathcal{D}^R_\lambda(\mathbf{q},\omega)=\sum_j A_{\lambda,j}(\mathbf{q})\left(\frac{1}{\omega-\Omega_{\lambda,j}(\mathbf{q})+i\delta}-\frac{1}{\omega+\Omega_{\lambda,j}(\mathbf{q})+i\delta}\right),\quad \delta\to+0, \tag{26}$$

where $A_{\lambda,j}(\mathbf{q})$ is the residue of $\mathcal{D}^R_\lambda(\mathbf{q},\omega)$ at $\omega=\Omega_{\lambda,j}(\mathbf{q})$. The Green's function $\mathcal{D}_\lambda(\mathbf{q},\omega)$ is obtained from $\mathcal{D}^R_\lambda(\mathbf{q},\omega)$ using relations between $\mathrm{Im}\,\mathcal{D}^R_\lambda(\mathbf{q},\omega)$ and $\mathrm{Im}\,\mathcal{D}_\lambda(\mathbf{q},\omega)$ similar to Eq. (22), and the Kramers-Kronig dispersion relations. As a result, the Green's function $\mathcal{D}_\lambda(\mathbf{q},\omega)$ can be written down explicitly,

$$\mathcal{D}_\lambda(\mathbf{q},\omega)=\sum_j \frac{A_{\lambda,j}(\mathbf{q})}{1-e^{-\beta\Omega_{\lambda,j}(\mathbf{q})}}\left(\frac{1}{\omega-\Omega_{\lambda,j}(\mathbf{q})+i\delta}+\frac{e^{-\beta\Omega_{\lambda,j}(\mathbf{q})}}{\omega+\Omega_{\lambda,j}(\mathbf{q})+i\delta}\right),\quad \delta\to+0. \tag{27}$$

It is seen from Eqs. (16) and (27), that the parameter

$$w_{\lambda,j}(\mathbf{q})\equiv|(\gamma_{\lambda,\mathbf{q}})_{11}|^2A_{\lambda,j}(\mathbf{q}) \tag{28}$$

determines the strength of the coupling between an electron and the $(\lambda,j)$-th magneto-plasmon-phonon mode characterized by the wave vector $\mathbf{q}$.

## III. RESULTS AND DISCUSSION

Using the method developed in the previous section, the magnetoplasmon-phonon frequencies and the magnetoabsorption spectra of a GaAs/AlAs quantum well are now calculated numerically. Within this approach, the CR peaks are proportional to $\delta$ functions because of the discrete energy spectrum of an electron in a quantum well in the presence of a magnetic field (see, e.g., Ref. 21). In what follows, we introduce in Eq. (16) a finite broadening $\gamma$ of the Landau levels instead of the infinitesimal parameter $\delta\to+0$. Here, we choose the value $\gamma=0.01\omega_{L1}$, which corresponds to the linewidth of the CR peaks in the experiment of Ref. 12. The material parameters used for the present calculation are listed in Table I. The value 0.915 eV (Ref. 21) is used for the AlAs/GaAs potential barrier. In the numerical calculation, we use a formula for the energy levels in a nonparabolic conduction band taken from Refs. 34, 35

TABLE I. Material parameters used for the calculation of the magnetoabsorption spectra of a GaAs/AlAs quantum well.

| Parameter | GaAs | AlAs |
|---|---|---|
| LO-phonon energy, meV | 36.3 (Ref. 12) | 50.09 (Ref. 37) |
| TO-phonon energy, meV | 33.6 (Ref. 12) | 44.88 (Ref. 37) |
| Electron band mass, in units of the electron mass in the vacuum | 0.0653 (Ref. 35) | 0.15 (Ref. 37) |
| High-frequency dielectric constant | 10.89 (Ref. 37) | 8.16 (Ref. 37) |
| Electron-phonon coupling constant | 0.068 (Ref. 3) | 0.148 (Ref. 37) |

$$E_{nl}=\frac{E^*_0}{2}\left(\sqrt{1+4\frac{E^0_{nl}}{E^*_0}}-1\right). \tag{29}$$

with the effective energy gap $E^*_0=0.98$ eV (Ref. 35) and with $E^0_{nl}=\hbar\omega_c(l+1/2)+\varepsilon_n$, where $\varepsilon_n$ is a size-quantized energy level characterizing the motion along the $z$ axis.

According to Ref. 21, the following phonon branches give contributions to the CR spectra in a quantum well: (i) bulk-like phonons with frequency $\omega_{L1}$ and (ii) symmetric interface phonons with frequencies $\omega_{S,\pm}(q)$ given by Eq. (7) of Ref. 21. In a similar way the magnetoplasmon-phonon modes in a quantum well can be classified into bulklike and interface modes. The frequencies of these modes depend on the electron density and on the modulus $q$ of the 2D wave vector $\mathbf{q}$. As follows from our calculations, the modes, whose wave vectors lie in the region with $q\sim 2q_p$, where $q_p\equiv(m_b\omega_{L1}/\hbar)^{1/2}$, give the dominant contribution to the magneto-optical absorption. In Fig. 1, frequencies of six mixed magneto-plasmon-phonon modes, which contribute significantly to the cyclotron-resonance spectrum, are plotted as a function of the electron density for $\omega_c=0.8\omega_{L1}$ and for $q=2q_p$. In the low-density limit, as seen from Fig. 1, the phonon modes do not mix with the magnetoplasmons. At $n_S\to 0$, the frequencies of the bulklike and of two symmetric interface magnetoplasmon-phonon modes tend to $\omega_{L1}$ and $\omega_{S,\pm}(q)$, respectively (see Ref. 21). With increasing density $n_S$, the magnetoplasmon branch splits into three modes (shown by heavy curves). When the density rises further, anticrossing of phonon and magnetoplasmon frequencies is to be expected between $10^{11}\ \mathrm{cm}^{-2}\lesssim n_S\lesssim 10^{12}\ \mathrm{cm}^{-2}$. This anticrossing allows us to distinguish between the lower-frequency modes (heavy curves) and the higher-frequency modes (thin curves). Finally, for $n_S\gtrsim 10^{12}\ \mathrm{cm}^{-2}$, the three higher frequencies tend to the magnetoplasmon frequency, which behaves as $\sim n_S^{1/2}$, and the three lower frequencies are close to $\omega_{T1}$ and to $\omega_{S,\pm}(q)$, respectively. The latter two magnetoplasmon-phonon frequencies are actually slightly reduced with respect to $\omega_{S,\pm}(q)$. The appearance of the branch

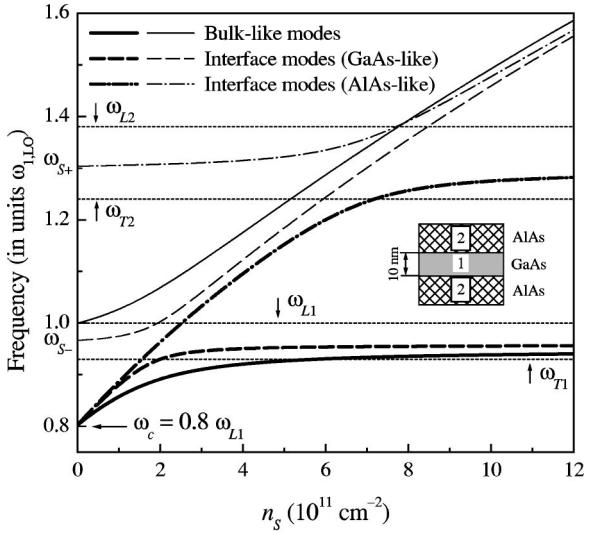


FIG. 1. Frequencies of magnetoplasmon-phonon modes in a 10-nm GaAs/AlAs quantum well as a function of the electron density. The value $\omega_c = 0.8\omega_{L1}$ is taken for the cyclotron frequency. Solid, dashed and dash-dotted curves correspond to bulklike, interface (GaAs), and interface (AlAs) modes, respectively.

with frequency close to $\omega_{T1}$ instead of $\omega_{L1}$ is due to the screening of the electron-phonon interaction by the plasma vibrations.

In Fig. 2, the relative contributions of different magnetoplasmon-phonon modes to the total magnetopolaron coupling strength

$$\tilde{w}_{\lambda,j}(q) \equiv \frac{w_{\lambda,j}(q)}{\Sigma_{\lambda,j} w_{\lambda,j}(q)} \tag{30}$$

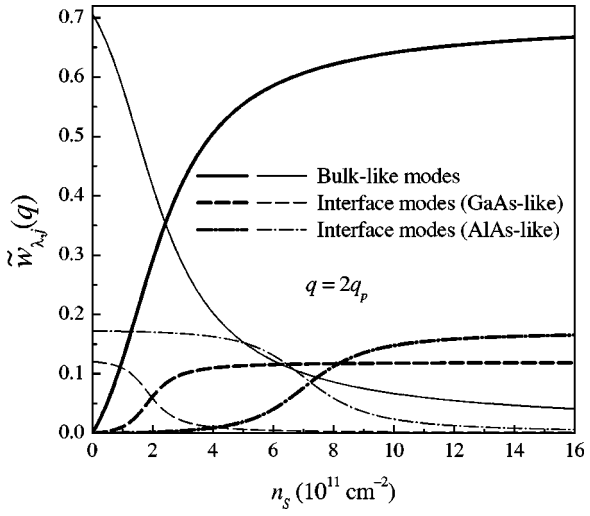


FIG. 2. Relative contributions of six magnetoplasmon-phonon modes to the total magnetopolaron coupling strength $w(q) \equiv \Sigma_{\lambda,j} w_{\lambda,j}(q)$ in a 10-nm GaAs/AlAs quantum well as a function of the electron density. The other modes are neglected, because their relative contribution is only about $10^{-4}$ of $w(q)$. The notations are the same as those of Fig. 1.

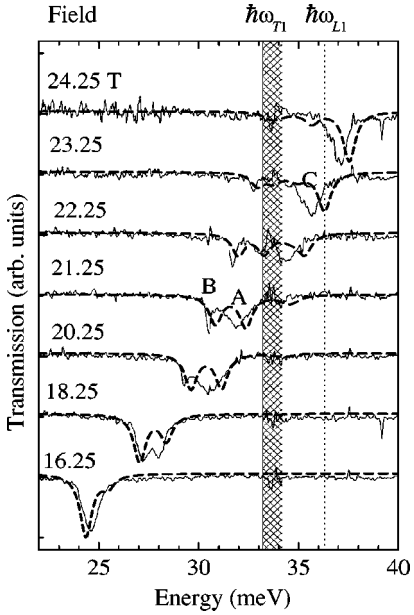


FIG. 3. Experimental and theoretical transmission spectra, at different magnetic fields, for a 10-nm GaAs/AlAs quantum well with electron density $n_S = 1.28 \times 10^{12}$ cm$^{-2}$. The solid curves represent the experimental data of Ref. 12. The dashed curves correspond to the present theory.

are plotted as a function of $n_S$ for $q = 2q_p$. In the low-density limit, the plasma vibrations give a vanishing contribution to $\tilde{w}_{\lambda,j}(q)$. In this case, the electrons interact only with phonons. For increasing electron density, the strength of the interaction of an electron with the lower-frequency magnetoplasmon-phonon modes rises, while that for the higher-frequency modes decreases. For a 10-nm GaAs/AlAs quantum well, the contribution of the interface magnetoplasmon-phonon modes into the CR spectra is smaller than that of the bulklike modes. Nevertheless, the interaction of an electron with the interface modes is not negligible.

It was noted in Refs. 38, 39, that the participation of a magnetoplasmon at $\mathbf{q} \neq 0$ in CR for a purely electronic system in a quantum well, without impurities, is not allowed by momentum conservation. However, for a polaron gas in a quantum well, the interaction of the electrons with the magnetoplasmon-phonon modes characterized in Fig. 2 is reflected in the CR spectrum. It is remarkable that in the high-density limit, the largest coupling strength occurs for the mixed magnetoplasmon-phonon mode with $\omega \approx \omega_{T1}$. This fact provides a quantitative basis for the understanding of the resonant magnetopolaron coupling observed in Ref. 12. A related effect appears also for the magneto-phonon resonance: as shown in Ref. 40, the magnetoplasmon-phonon mixing leads to a shift of the resonant frequency of the magnetophonon resonance in quantum wells from $\omega \approx \omega_{L1}$ to $\omega \approx \omega_{T1}$.

In Ref. 12, CR spectra are measured for the absolute transmission $T(\omega)$, which is related to the optical absorption coefficient by

$$T(\omega) \equiv 1 - \Gamma(\omega). \tag{31}$$

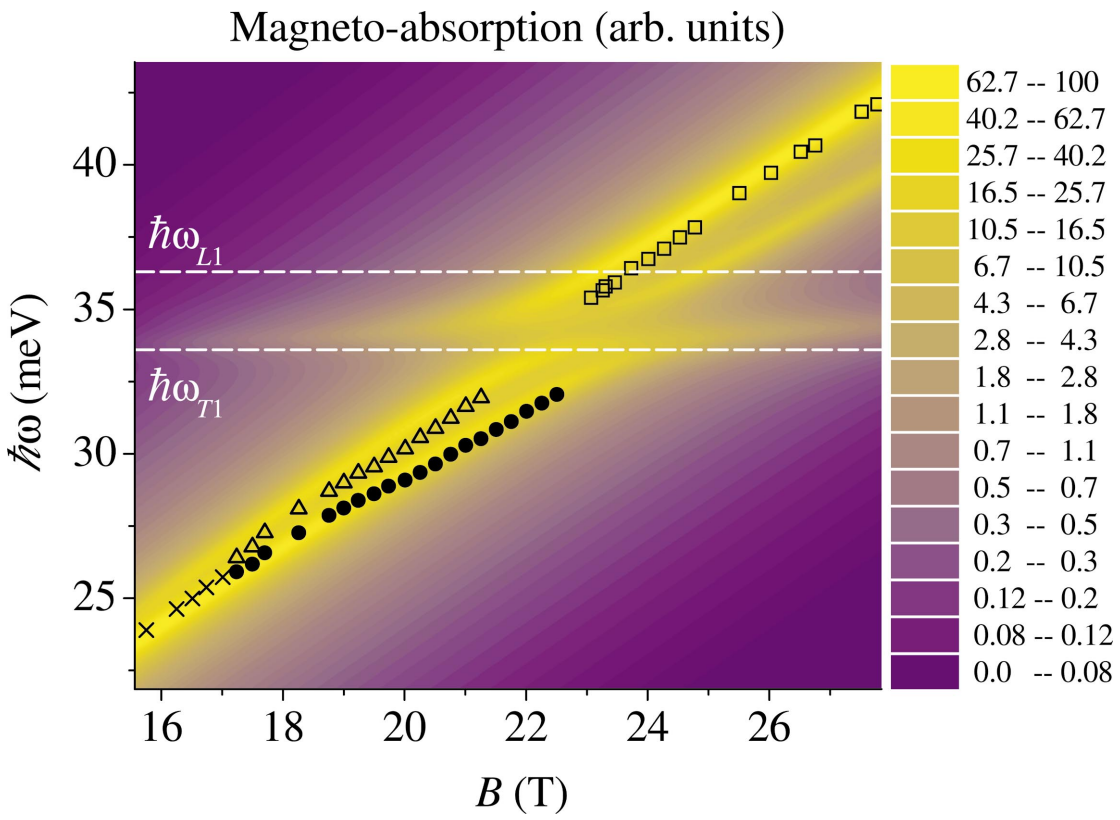


FIG. 4. (Color) Color map of the cyclotron resonance spectra for a 10-nm GaAs/AlAs quantum well. Symbols indicate the peak positions of the experimental spectra (which are taken from Fig. 3 of Ref. 12). The dashed lines show LO- and TO-phonon frequencies in GaAs.

The optical absorption coefficient is proportional to Re $\sigma(\omega)$,

$$\Gamma(\omega)=\frac{4\pi}{cn(\omega)}\,\mathrm{Re}\,\sigma(\omega), \tag{32}$$

where $n(\omega)$ is the refractive index. In Fig. 3, we compare the experimental[12] transmission spectra with the transmission spectra calculated in the present work for a polaron gas with electron density $n_S=1.28\times10^{12}$ cm$^{-2}$ in a 10-nm GaAs/AlAs quantum well. Reliable comparison of our theoretical results with the experimental data of Ref. 12 can be performed only outside a frequency band near $\omega_{T1}$ (shown in Fig. 3 by the cross-hatched area), because the experimental spectra in this frequency region are obtained after the elimination of a strong absorption peak due to direct TO-phonon absorption in the substrate. It is not straightforward to extract information on the CR spectra in this frequency region. It is seen from Fig. 3, that outside the cross-hatched area the theoretical peak positions of the magnetotransmission spectra calculated in the present work reasonably compare with the experimental data of Ref. 12. If one tunes the magnetic field within the error bar, the agreement between theory and experiment can be improved. The remaining difference between theoretical and experimental peak positions can be explained by possible deviation of the values of the band parameters (the electron band mass and the effective energy gap) in a GaAs/AlAs quantum well from those in bulk.

The effect of the magnetoplasmon-phonon mixing is clearly manifested in the CR spectra, as seen, e.g., from the plot corresponding to a magnetic field $B=22.25$ T, for which $\omega_c\approx\omega_{T1}\approx33.6$ meV. For this value of $B$, the intensities of the peaks below $\omega_{T1}$ and above $\omega_{T1}$ are comparable both in the experiment[12] and in the present theory. Such a behavior is typical for resonant magnetopolaron coupling near $\omega_{T1}$ rather than near $\omega_{L1}$.

The splitting of the CR peaks manifested in Fig. 3 reflects the nonparabolicity of the conduction band. In the experimental CR spectra,[12] the higher-frequency and lower-frequency components of the split peaks are denoted as $A$, respectively, $B$ components. The higher-frequency component of each split peak corresponds to the transitions between the Landau levels $(0\rightarrow1)$, while the lower-frequency component corresponds to the transitions $(1\rightarrow2)$. With increasing magnetic field strength, the distance between Landau levels rises, so that the upper filled level $(l=1)$ becomes less populated. As a result, the relative intensity of the lower-frequency peak diminishes. It is shown in Ref. 16, that the observed relative oscillator strengths of the split CR peaks are not consistent with the one-particle theoretical picture. The one-particle theories (e.g., Refs. 41, 42) overestimate the lower-frequency peak intensity as compared to experiment. In particular, for a filling factor $\nu=3$, the one-particle approximation predicts $I_{(1\rightarrow2)}/I_{(0\rightarrow1)}\approx2$, which contradicts the experimental CR data for high electron densities,[16] where this ratio is close to 1. It is noteworthy, that for $\nu=3$, the coefficients $\varkappa_{nl\sigma}$ given by Eq. (15) for $l=0$ and for $l=1$ are equal to each other, while the contributions Re $\sigma_{nl\sigma}(\omega)$ only

slightly depend on the Landau level quantum number. Therefore, for $\nu=3$, our theory gives $I_{(1\to2)}/I_{(0\to1)}\approx1$, in agreement with Ref. 16.

In Fig. 4, we plot a set of our theoretical magnetoabsorption spectra for a GaAs/AlAs quantum well as a color map. This map shows the magnetoabsorption intensity as a function of both the magnetic field and the frequency. For comparison, the experimental peak position taken from Fig. 3 of Ref. 12 are shown in the same graph. For the peaks with $B \ll 17.2$ T (indicated by crosses) the splitting due to the band nonparabolicity is not resolved experimentally. It is seen from Fig. 4 that, for the high-density electron gas, anticrossing of the CR spectra occurs near $\omega_{T1}$ both for the experimental and for the calculated CR spectra. Starting from large $B$, a set of peaks with $\omega>\omega_{T1}$ are pinned towards $\omega_{T1}$ from above, while starting from $B\sim0$, another set of peaks are pinned from below to a frequency slightly larger than $\omega_{T1}$.

For a low-density polaron gas in a GaAs/AlAs quantum well, it was found[21] that the resonance frequencies, calculated taking into account the interaction of electrons with both bulklike and interface phonons, appreciably deviate from those found for the interaction with bulk LO phonons only. In particular, due to interface phonons, a resonance frequency appears between $\omega_{L1}$ and $\omega_{T1}$ (see Fig. 7 of Ref. 21). In the present work, we take into account, in addition to the effects due to the interaction of electrons with bulklike and interface phonons, the many-body effects, which ensure the shift of the resonance frequency towards $\omega_{T1}$, when the electron density is high enough.

The splitting of the magnetoabsorption peaks due to the band nonparabolicity, observed in the experiment for $\omega<\omega_{T1}$, continues in the theoretically calculated spectra also in the region $\omega>\omega_{T1}$. However, the intensity of the $B$ component for $\omega>\omega_{T1}$ is quite small.

## IV. CONCLUSIONS

We have theoretically investigated cyclotron-resonance spectra for a polaron gas in a GaAs/AlAs quantum well with high electron density, taking into account (i) the electron-electron interaction and as a consequence the screening of the electron-phonon interaction, (ii) the magnetoplasmon-phonon mixing, (iii) the electron-phonon interaction with relevant phonon modes specific for the quantum well under consideration. As a result of the mixing, different magnetoplasmon-phonon modes appear in the quantum well and contribute to the CR spectra. In the 10-nm GaAs/AlAs quantum well (investigated experimentally in Ref. 12), the interaction of an electron with the bulklike modes is dominant. It is shown in the present work that, in the high-density polaron gas, the resonant magnetopolaron coupling, manifested in the CR spectra, takes place at a frequency close to the TO-phonon frequency in GaAs. This effect is in contrast with the cyclotron resonance of a low-density polaron gas in a quantum well, where anticrossing occurs near the LO-phonon frequency. Due to the band nonparabolicity, the CR spectrum of a high-density polaron gas in a quantum well is split into two components. The calculated CR spectra are in agreement with experiment, in particular, with the results of Ref. 12.

## ACKNOWLEDGMENTS

Discussions with V. M. Fomin, G. Martinez, and V. N. Gladilin are gratefully acknowledged. This work has been supported by the GOA BOF UA 2000, I.U.A.P., F.W.O.-V. projects No. G.0274.01N, G.0435.03, the W.O.G. WO.025.99 (Belgium) and the European Commission GROWTH Program, NANOMAT project, Contract No. G5RD-CT-2001-00545.

*Permanent address: Department of Theoretical Physics, State University of Moldova, str. A. Mateevici 60, MD-2009 Kishinev, Republic of Moldova.

†Also at: Technische Universiteit Eindhoven, P. B. 513, 5600 MB Eindhoven, The Netherlands.

[1] *Polarons and Excitons*, edited by C. G. Kuper and G. D. Whitfield (Oliver and Boyd, Edinburgh, 1963).

[2] J. Appel, in: *Solid State Physics*, edited by F. Seitz, D. Turnbull, and H. Ehrenreich (Academic Press, NY, 1968), Vol. 21, pp. 193–391.

[3] *Polarons in Ionic Crystals and Polar Semiconductors*, edited by J. T. Devreese (North-Holland, Amsterdam, 1972).

[4] J. T. Devreese, in *Encyclopedia of Applied Physics* (VCH, Weihheim, 1996), Vol. 14, p. 383.

[5] P. Calvani, *Optical Properties of Polarons* (Editrice Compositori, Bologna, 2001).

[6] D. Larsen, Phys. Rev. A **135**, A419 (1964); in Ref. 3 p. 237.

[7] B. D. McCombe and R. Kaplan, Phys. Rev. Lett. **21**, 756 (1968).

[8] Y.-H. Chang, B. D. McCombe, J.-M. Mercy, A. A. Reeder, J. Ralston, and G. A. Wicks, Phys. Rev. Lett. **61**, 1408 (1988).

[9] J. P. Cheng, B. D. McCombe, and G. Brozak, Phys. Rev. B **43**, 9324 (1991).

[10] F. M. Peeters, X. Wu, J. T. Devreese, C. J. G. M. Langerak, J. Singleton, D. J. Barnes, and R. J. Nicholas, Phys. Rev. B **45**, 4296 (1992).

[11] M. Ziesmann, D. Heitmann, and L. L. Chang, Phys. Rev. B **35**, 4541 (1987).

[12] A. J. L. Poulter, J. Zeman, D. K. Maude, M. Potemski, G. Martinez, A. Riedel, R. Hey, and K. J. Friedland, Phys. Rev. Lett. **86**, 336 (2001).

[13] A. H. MacDonald and C. Kallin, Phys. Rev. B **40**, 5795 (1989).

[14] C. M. Hu, E. Batke, K. Köhler, and P. Ganser, Phys. Rev. Lett. **75**, 918 (1995).

[15] C. M. Hu, T. Friedrich, E. Batke, K. Köhler, and P. Ganser, Phys. Rev. B **52**, 12 090 (1995).

[16] M. Manger, E. Batke, R. Hey, K. J. Friedland, K. Köhler, and P. Ganser, Phys. Rev. B **63**, 121203 (2001).

[17] Yu. A. Bychkov and G. Martinez, Phys. Rev. B **66**, 193312 (2002).

[18] Wu Xiaoguang, F. M. Peeters, and J. T. Devreese, Phys. Rev. B **36**, 9760 (1987).

[19] H. Mori, Prog. Theor. Phys. **33**, 423 (1965); **34**, 399 (1965).

[20] F. A. P. Osório, M. H. Degani, and O. Hipólito, Phys. Rev. B **38**, 8477 (1988).

[21] G. Q. Hai, F. M. Peeters, and J. T. Devreese, Phys. Rev. B **47**, 10 358 (1993).

[22] G. Q. Hai, F. M. Peeters, and J. T. Devreese, Physica B **184**, 289 (1993).
[23] Y. J. Wang, H. A. Nickel, B. D. McCombe, F. M. Peeters, J. M. Shi, G. Q. Hai, X.-G. Wu, T. J. Eustis, and W. Schaff, Phys. Rev. Lett. **79**, 3226 (1997).
[24] J. T. Devreese and F. M. Peeters, in *High Magnetic Fields in Semiconductor Physics II*, edited by G. Landwehr, Vol. 87 of *Springer Series in Solid-State Sciences* (Springer Verlag, Heidelberg, 1989).
[25] N. Mori and T. Ando, Phys. Rev. B **40**, 6175 (1989).
[26] M. H. Degani and O. Hipólito, Surf. Sci. **196**, 459 (1988).
[27] M. H. Degani and O. Hipólito, Superlattices Microstruct. **5**, 141 (1989).
[28] G. Q. Hai, F. M. Peeters, and J. T. Devreese, Phys. Rev. B **42**, 11 063 (1990).
[29] L. Wendler and R. Pechstedt, J. Phys.: Condens. Matter **2**, 8881 (1990).
[30] E. P. Pokatilov, S. I. Beril, and V. M. Fomin, Phys. Status Solidi B **147**, 163 (1988).
[31] E. P. Pokatilov, S. I. Beril, V. M. Fomin, and V. V. Kalinovskii, Phys. Status Solidi B **161**, 603 (1990).
[32] E. P. Pokatilov, V. M. Fomin, and S. I. Beril, *Vibrational Excitations, Polarons and Excitons in Multilayer Structures* (Ştiinţa, Chişinău, 1990).
[33] D. Larsen, Phys. Rev. B **35**, 9301 (1987).
[34] X. Wu, F. M. Peeters, and J. T. Devreese, Phys. Rev. B **40**, 4090 (1989).
[35] P. Pfeffer and W. Zawadzki, Phys. Rev. B **53**, 12 813 (1996).
[36] W. H. Backes, F. M. Peeters, F. Brosens, and J. T. Devreese, Phys. Rev. B **45**, 8437 (1992).
[37] S. Adachi, J. Appl. Phys. **58**, R1 (1985).
[38] C. Kallin and B. I. Halperin, Phys. Rev. B **31**, 3635 (1985).
[39] B. Zhang, M. F. Manger, and E. Batke, Phys. Rev. Lett. **89**, 039703 (2002).
[40] V. V. Afonin, V. L. Gurevich, and R. Laiho, Phys. Rev. B **62**, 15 913 (2000).
[41] K. L. Kobayashi and E. Otsuka, J. Phys. Chem. Solids **35**, 839 (1974).
[42] T. Ando, J. Phys. Soc. Jpn. **38**, 989 (1975).